Journal of Alloys and Compounds 848 (2020) 156494

Contents lists available at ScienceDirect

Journal of Alloys and Compounds

journal homepage: http://www.elsevier.com/locate/jalcom

A comparison of the microstructures, thermal and mechanical properties of pressed and sintered Ti–Cu, Ti–Ni and Ti–Cu–Ni alloys intended for dental applications

C. Machio [a, *], M.N. Mathabathe [a, b], A.S. Bolokang [a, c]

[a] Council for Scientific Industrial Research, Manufacturing Cluster, Advanced Materials and Engineering, Meiring Naude Road, P O Box 395, Pretoria, South Africa
[b] Department of Material Science and Metallurgical Engineering, Faculty of Engineering, Built Environment and Information Technology, University of Pretoria, South Africa
[c] Department of Physics, University of the Western Cape, P. O. Box 339, Private Bag X 17, Bellville, 7535, South Africa

ARTICLE INFO

Article history:
Received 7 May 2020
Received in revised form
26 June 2020
Accepted 21 July 2020
Available online 1 August 2020

Keywords:
Titanium-copper-nickel
Powder metallurgy
Mechanical properties
Dental
Thermal analysis
EBSD

ABSTRACT

The effect of Ni and Cu on the α→β phase transformation temperature, possible retention of the β-phase, and mechanical properties of Ti, Ti–13Cu, Ti–4.5Ni and Ti–13Cu–4.5Ni (compositions in wt. %) alloys were investigated. The alloys were developed using the conventional uniaxial cold press and sintering technique. The thermal properties of the sintered alloys were traced by the differential scanning calorimetry (DSC) analysis. The x-ray diffraction (XRD) and electron backscatter diffraction (EBSD) analysis determined phase composition, crystal structures and grain orientations. It has emerged that the Ti–13Cu and Ti–13Cu–4.5Ni retained the β-Ti phase. The mechanical properties were evaluated under tension with Ti–13Cu and Ti–4.5Ni possessing high ultimate tensile strength (UTS) and percentage elongation (%El) than the Ti–13Cu-4.5Ni alloy. Although all the alloys have revealed the presence of porosity, its effect on mechanical properties was more on the Ti–13Cu–4.5Ni alloy. While the mechanical properties of Ti–13Cu-4.5Ni alloy were inferior due to extensive porosity, those of Ti, Ti–13Cu and Ti–4.5Ni allow them to be classified as Type 3 and Type 4 dental alloys, respectively, proving that the conventional powder metallurgy process has potential to be used as a processing technique for Ti–Cu-based dental alloys.

1. Introduction

Titanium-based alloys specifically those containing nickel (Ni) and copper (Cu) alloying are attractive for the dental industry. For example, high Ni content Ti–Ni alloys have been commonly used for a wide variety of industrial fields because of their shape memory effect (SME) [1]. Dental applications benefit from the shape memory effect, biocompatibility, low modulus of elasticity (MOE), corrosion and fatigue resistance, and high damping capacity [2]. In particular, the Ti–Ni shape memory alloy (SMA) has been used as orthodontic wire since the early 1980s [3]. The addition of copper (Cu) to the Ti–Ni shape memory alloys (SMA) modifies their shape memory behaviour, making Cu–Ti–Ni SMA orthodontic wires easier to apply in dentistry than the Ti–Ni SMA wires [3,4]. The Cu also improves the corrosion resistance of the Ni–Ti SMA and other biomedical properties such as antibacterial function [5].

Cast binary Ti–Cu alloys have been extensively investigated for application as dental alloys. The anti-bacterial property is attributed to the release of Cu^{+2} ions from the Ti_2Cu intermetallic compounds which form in the alloys. The anti-bacterial properties have been demonstrated by, for example, Liu et al. [5] who showed that a vacuum melted Ti-5wt% Cu alloy eliminates and inhibits adhesion and biofilm formation of the bacteria *Streptococcus mutans* and *Porphyromonas gingivalis* that can occur in the human mouth. It has been suggested that high Cu-contents are especially promising because they improve the anti-bacterial properties [6], but that is up to a point, because while contents as high as 25 wt% Cu can possess as good biocompatibility as that of pure cp-Ti [7], much higher contents (50–60 wt% Cu) are not biocompatible [8]. The Ti–Cu alloys are amenable to thermomechanical processing, e.g.

* Corresponding author.
E-mail addresses: cmachio@csir.co.za (C. Machio), nmathabathe@csir.co.za (M.N. Mathabathe), sbolokang@csir.co.za (A.S. Bolokang).

https://doi.org/10.1016/j.jallcom.2020.156494
0925-8388/

hot extrusion, which increases their hardness, compressive yield strength and enhances the corrosion resistance significantly without affecting the antibacterial properties due to fine Ti_2Cu [9]. These properties make the Ti—Cu alloys not only suitable for dental applications but also other biomedical applications.

Elemental Ni is a ferromagnetic metal that transforms into the paramagnetic state upon thermal treatment. This magnetic phase transition is known as the second-order phase transition also affected by mechanical deformation [10,11]. Ni release to human body cells is regarded as toxic. However, the wear or corrosion of Ni ions is restrained by alloying with Ti (TiNi). Moreover, the formation of a protective passive film on the surface of the Ti~50 at. %Ni consisting of TiO_x oxides with a small amount of NiO inhibits the Ni ions released to the human body [12]. This alloy is preferable for biomedical application due to low elastic modulus of 48 GPa close to that of a human bone (~30 GPa) and offers enhanced biocompatibility and superplasticity [13]. Apart from conferring shape memory properties to Ti for use in orthodontic wires, it (Ni) is also extensively used as high nickel content, cast nickel-chromium (Ni—Cr) alloys for commercial clinical prosthodontic restorations [14,15]. While the release of Ni ions from dental alloys is a matter of concern, because Ni ions cause allergenic responses, risk severe local tissue irritation, necrosis, and toxic reactions [16], and can, depending on concentration, be toxic and non-compatible [17], its continued use is generally still safe because it has been shown that Ni release from the alloys is orders of magnitude less than the allowable daily dietary intake [8,18,19], and the released ions decrease only the proliferation of human gingival fibroblast cells, not their viabilities [14]. Some studies on commercial partial dentures based on Ni (Ticonium) have found them to be biocompatible when tested against fibroblasts (Balb/c 3T3 cells) [8].

The Ti—13Cu-4.5Ni alloy has been investigated for use as cast crowns and partial denture frameworks [20], and, novel Ti—Ni—Cu shape memory alloys, possessing good anti-bacterial properties have been developed in recent years [21].

The presence of both Cu and Ni improves the ease of casting of the alloy by enabling melting at lower temperatures [22] and inducing more liquid phase at the processing temperature. The alloy is more corrosion resistant than the other dental alloys like the Ni—Cr-based alloys [23]. Ni, like Cu, is expected to cause solid solution strengthening of Ti, improving its mechanical properties since un-alloyed Ti is generally not strong enough for some applications. Ni is also expected to further improve the antibacterial properties of the alloys, given their level of toxicity to cells is about the same [24].

The current manufacturing technique for dental alloys is casting [8,25]. However, the properties of cast Ti-based alloys can be immensely affected by the investment material used on the moulds: the molten melt tends to react with the investment material leading to compromised mechanical properties [26]. Besides, cast Ti-xCu alloys show an increase in elastic modulus with Cu content due to the formation of Ti_2Cu intermetallic phase [27]. Their phase composition consists of the Ti_2Cu intermetallic phase in lamellae eutectoid structure and as a single grain in the grain boundaries of the cast alloys containing 10% or more Cu, and remains unchanged with no visible β-phase even with increasing Cu content up to 20 wt% [28]. These shortcomings of casting can be avoided by changing the manufacturing process to powder metallurgy (PM), followed by further processing to final shape. There are many PM techniques, including the conventional press and sinter (CP&S), hot press (HP) and cold/hot isostatic pressing (C/HIP).

The research group of Erlin Zhang et al. [29] has done some work on hot pressing of Ti—Cu alloys, where powder blends are processed at high temperature and under pressure. Their work has indicated that hot-pressed Ti—Cu powder metallurgy alloys still possess their anti-bacterial properties found in the cast alloys, however, the antibacterial property required a Cu content of at least 5 wt% [30]. However, hot pressing, while it provides components with improved properties, requires a huge capital outlay on equipment, is generally energy in-efficient and results in high manufacturing costs [31]. A much more energy-efficient and low-cost manufacturing process is the conventional press and sinter (CP&S) powder metallurgy technique where compacted powder blends are processed at high temperature only, i.e. without pressure. To the best knowledge of the authors, much less research has been done on processing these potential dental alloys using the CP&S powder metallurgy technique. Luangvaranunt and Pripanapong's [32] work only investigated the wear behaviour of Ti—(2 &10)Cu wt% alloys processed by CP&S and showed that a high Cu content was good for wear resistance. Alshammari et al. [19] have recently reported only on the mechanical properties of forged CSP&S Ti—Cu alloys with up to, 5 wt% Cu. There is no known work yet on the CP&S of high Cu content Ti—Cu or Ti—Cu—Ni alloys. Such work has the potential of indicating the possibility of producing low-cost dental implants while at the same time, providing insight into the microstructures and phases of the alloys. For example, investigations have shown that titanium alloys containing the β-phase are good for orthopaedic prosthesis implants due to their low elastic modulus compared to CP Ti [13], yet it is not clear whether the β-phase occurs in these potential dental alloys when processed by CP&S. Moreover, alloys containing porous structures, like those prepared by CP&S, are also favourable for good biocompatibility and cell growth associated with further reduced elastic modulus [33], yet it is not clear whether these porous alloys can possess similar mechanical properties to those of the established dental alloys. Generally, the mechanical properties are of interest because they determine formability and wear resistance [34] and application as dental clasps, dental bridges or partial dentures [35].

The current study investigated conventionally pressed and sintered Ti—13Cu, Ti-4.5Ni, and Ti—13Cu-4.5Ni (all compositions in wt. %). The latter composition was chosen for ease of processing since it is expected that the presence of both Cu and Ni will enable melting at lower temperatures and induce more liquid phase at the processing temperature. The phase formations, phase transformations and mechanical properties were determined. For comparison purposes, commercially pure Ti (cp-Ti) was also processed for analysis.

2. Experimental work

2.1. Powders

Powder blends of commercially pure Ti, Copper, and Nickel were made by weighing required compositions accurately using a scale with an accuracy of 0.1 mg. The mixtures were then blended in a Turbular® mixture for 30 min to produce homogeneous blends. The Ni powder is similar to the one used in a previous related study [36]. Fig. 1 shows the morphologies of the elemental powders, and Table 1 summarizes their relevant details. The powder particle size distributions quoted in Table 1 are those provided by the respective suppliers, and while, for example, Ti powder is quoted as having powder particles less than 88 μm, statistically, some particles are expected to be larger than 88 μm.

2.2. Blended powder consolidation

The blended powders of Ti—13Cu, Ti-4.5Ni and Ti—13Cu-4.5Ni (all masses in wt%), were consolidated at 600 MPa using a conventional uni-axial press to produce green compacts, a similar technique is reported elsewhere [37]. Three sets of green compacts

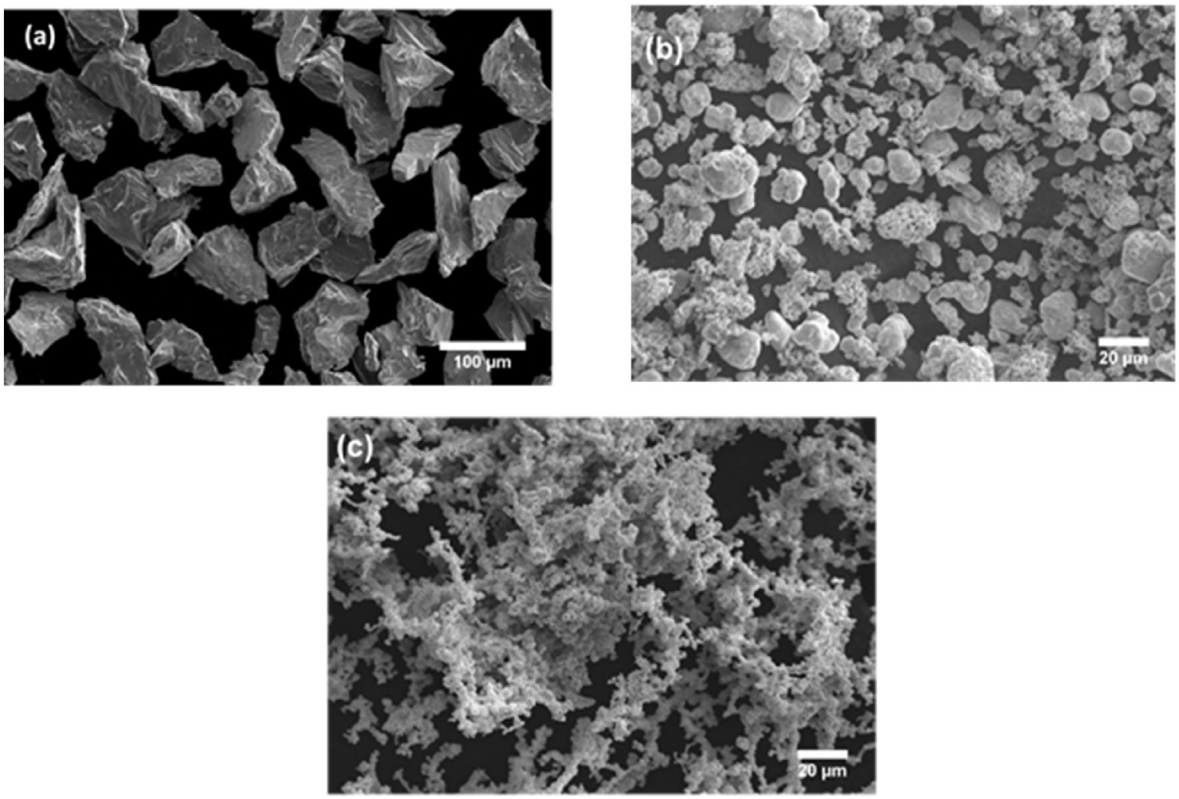

Fig. 1. Morphology of the metallic powders: (a) Ti, (b) Cu, and (c) Ni.

Table 1
Raw materials as specified per supplier.

Powders	Purity (%)	Morphology	Particle size distribution (µm)	Supplier
Ti	99.9	Irregular	−88	PAC, USA
Cu	99.97	Irregular + Spherical agglomeration	−75	Sigma Aldrich©
Ni	99.95	Fibrous-dendritic	−45	Sigma Aldrich©

were produced per alloy, one consisting of specimens of diameter 15 mm and thickness 4 mm was for determining density, microstructures, phase composition and hardness, while the other set consisted of specimens 10 × 10 × 50 mm, for determining the mechanical properties.

All the green compacts were sintered in a tube furnace under flowing argon. Specimens were heated up at a rate of 10°/min up to the sintering temperature of 1200 °C, soaked for 3 h, followed by furnace cooling. In order to avoid specimen oxidation, titanium sponge particles were loaded alongside the specimens to act as oxygen getters, i.e., to remove any oxygen in the argon gas before reaching the specimens.

2.3. Characterisation of sintered compacts

The sintered specimens were characterized for thermal behaviour, density, microstructures, hardness number and mechanical properties. The thermal behaviour was investigated using differential scanning calorimetry (DSC)/thermogravimetric analysis (TGA) tests, in a Netzsch STA 409 thermal analyser, capable of simultaneously capturing calorimetric and thermogravimetric signals. Samples were heated to 1300 °C at 10 °C/min under argon. The densities were determined as an average of three from different samples. Each density was determined using Archimedes principle according to ASTM B 962−08, the Standard Test Methods for Density of Compacted or Sintered Powder Metallurgy (PM) Products Using Archimedes' Principle. Masses were measured using a scale of accuracy 0.1 mg.

The microstructures were acquired using a Leica optical microscope and a JEOL 6550 scanning electron microscope after metallographic sample preparation. Orientation information was investigated using electron backscatter diffraction (EBSD), and its data acquisition and analysis was performed by HKL Chanel 5 software. The EBSD sample preparation was performed according to the work done by Mathabathe et al. [38]. The orientations were measured in both the axial and radial directions of the specimens. The samples were ground and polished according to ASTM standard E3-11, employing diamond suspension (1 µm), subsequent to 50 nm colloidal silica [37], before hardness testing. Six samples per test for each alloy were prepared to validate the repeatability. Hardness numbers were determined using a Vickers hardness testing machine. The load used was 5 kgf, and the test involved a dwell time of 10 s. Five indents were made and the hardness expressed as an average. Rectangular tensile test specimens, 2 mm thick, 5 mm wide and 50 mm long were cut from the 10 × 10 × 50 mm sintered samples using electro-discharge machining (EDM), to have a gauge length of 25 mm long and a width of 2.5 mm in the reduced section (Fig. 2). An Instron 1342

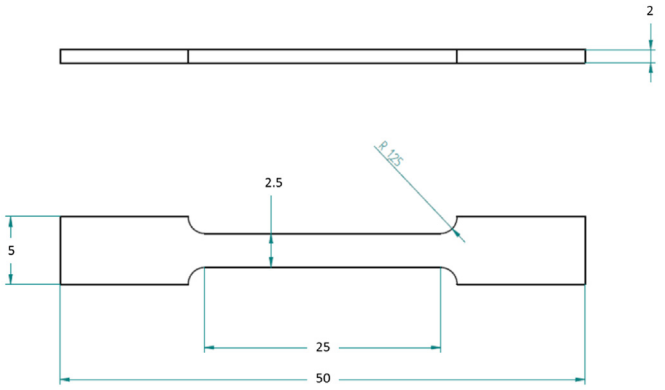

Fig. 2. The dimensions of the tensile test specimens.

Servo-Hydraulic tester was utilised to conduct tensile tests using a crosshead speed of 0.5 mm/min. Mechanical extensometer was also used to track deformation behaviour. The yield point, determined using the offset method, ultimate tensile strength, and the elongation to failure were reported as averages of three samples. All the test specimens failed within the gauge length, away from the fillet radii, and were deemed acceptable.

3. Results and discussion

3.1. Thermal behaviour

Fig. 3 shows the thermal behaviour of the conventionally pressed and sintered Ti, Ti−13Cu, Ti-4.5Ni, and Ti−13Cu-4.5Ni alloys as determined using DSC-TGA analysis. The thermal behaviour of Alloy 1, the cp-Ti samples, had an endothermic peak centred at 914 °C, which was attributed to the α (hcp) → β (bcc) Ti allotropic transformation. Alloying with Cu and Ni changed this behaviour, due to the formation of intermetallic phases, as the following sections show.

3.1.1. The Ti−Cu thermogram

The introduction of Cu alone, in Alloy 2, Ti−13Cu, led to two profound endothermic peaks in the Ti−Cu thermogram (Fig. 3), one centred at 824.9 °C, with an end temperature of 851 °C representing the completion of the eutectoid reaction where α-Ti reacts with some Ti_2Cu to form β-Ti, i.e. α-Ti + Ti_2Cu → β-Ti. The second endothermic peak is centred at 932 °C, with an end temperature at 950.9 °C and is attributed to the simultaneous melting of Ti_2Cu + TiCu, which occurs at 960 °C on the Ti−Cu phase diagram [19]. The exothermic peak at 1006.8 °C is likely due to the eutectic reaction Ti_2Cu + β-Ti → L, and the subsequent dissolution of β-Ti in the resulting melt. The reaction is exothermic because the dissolution of β-Ti in copper-containing melts is an exothermic process [39]. This thermal behaviour indicated that the possible phases in the sintered Ti−13Cu alloy were α-Ti, TiCu, and Ti_2Cu.

3.1.2. Ti−Ni thermogram

The thermogram of Ti-4.5Ni binary alloy reveals an endothermic α→β Ti phase transformation peak at 773 °C. It is evident that 4.5 wt % Ni content affects the α→β phase transformation temperature of Ti. After the transformation, the occurrence of the eutectoid reaction αTi + Ti_2Ni → βTi, which is indicated to occur at 767 °C on the Ti−Ni phase diagram [40−43]. No further phase changes were observed because any Ti_2Ni was wholly consumed by the eutectoid reaction. The Ni content used in the alloy was lower than the eutectoid Ni composition (~8.4 wt %) [42,43] and further temperature increases remained in the β-Ti phase field.

3.1.3. Ti−Cu−Ni thermogram

The Ti−13Cu-4.5Ni thermograph had three endothermic and one exothermic complex peaks. The first endothermic peak is centred at around 762 °C, and combines a peak at 734 °C, which

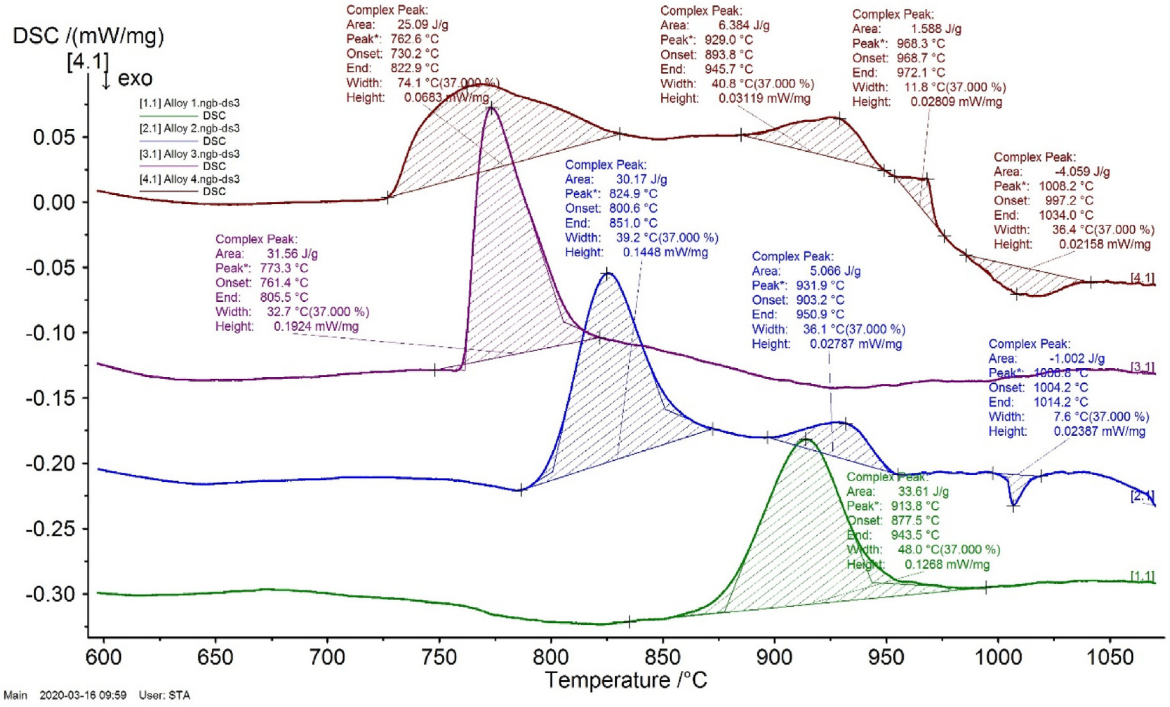

Fig. 3. The thermograms of the specimens DSC analysis of the sintered Ti (Alloy 1), Ti−13Cu (Alloy 2), Ti-4.5Ni (Alloy 3) and Ti−13Cu-4.5Ni (Alloy 4) alloys.

could be attributed to the ternary eutectoid reaction α-Ti + Ti_2Ni + Ti_2Cu → β-Ti [42], while the peaks at 768 °C and 812 °C are due to the binary eutectoid reactions α-Ti + Ti_2Ni → β-Ti and α-Ti + Ti_2Cu → β-Ti, respectively, indicating that the complex peak is due to the formation of β-Ti phase. The second endothermic peak is centred at 929 °C and combines a peak at 913 °C, which could be attributed with the reaction Ti_2Ni + Ti_2Cu → β-Ti + L [43], and a peak at 925 °C, associated with the eutectic reaction β-Ti + Ti_2Ni → L in the Ti–Ni system [20]. The last endothermic peak is centred at 969 °C could be associated with the formation of a liquid phase due to the peritectic reaction Ti_2Ni + Ti_2Cu → β-Ti + L [44]. The exothermic peak is centred at 1008 °C, and could be associated with the eutectic reaction β-Ti + Ti_2Cu → L, as occurs in the Ti–Cu system [19]. As already indicated for the Ti–13Cu alloy, the reaction is exothermic because the dissolution of β-Ti in copper-containing melts is an exothermic process [39].

3.2. Microstructure characterisation

3.2.1. Optical microstructures

The optical microstructures (Fig. 4) showed that all the alloys investigated were porous. Only the polished micrograph for Alloy 1 (CP–Ti) is shown (Fig. 4 a) because the microstructure consisted only of the usual α-Ti grains. The microstructure of Alloy 3 (Ti-4.5Ni) had bright elongated pro-eutectoid α-Ti laths/plates, and dark domains, which were un-resolvable in the optical microscope (Fig. 4 c). Similar microstructures have been reported in the literature, for low Ni content Ti–Ni alloys processed by spark plasma powder metallurgy technique [45]. On the other hand, the microstructures of the Cu-containing alloys {Alloy 2 (Ti–13Cu) (Fig. 4 b)} and {Alloy 4 (Ti–13Cu-4.5Ni) (Fig. 4 d)} are composed of pro-eutectoid dark-coloured precipitates having either blocky/globular, elongated plate-like or sometimes, dendritic, morphologies, and regions consisting of a mixture of a bright phase and elongated dark-coloured precipitates. The microstructures also contained "pearlitic" regions due to the eutectoid reactions. The mixed phases in Ti–13Cu are mostly lamellar nodules but in some areas, the spherules were observed, where the elongated dark-coloured precipitates grew radially from the centres. Unlike Ti–13Cu, no spherules were observed in Ti–13Cu-4.5Ni alloy.

3.2.2. SEM microstructures

Fig. 5 shows characteristic SEM secondary electron (SE) micrographs of the alloys 2, 3 and 4. Fig. 5 (a) and (b) clearly shows the different morphologies of the precipitates (dendritic and blocky/globular) and the lamellar and "spherulitic" "pearlitic domains in Alloy 2 (Ti–13Cu). These "spherulitic" domains observed here were similar to the blocky nodules observed in a cast Ti-12at.% Cu alloy that had been solution treated and soaked in the β-Ti phase-field where they formed by cellular decomposition mode [46]. EDS analysis of the precipitates in Alloy 2 confirmed Cu content of 27–30 at. %, justifying the presence of Ti_2Cu precipitates.

The SEM micrographs of Alloy 3 (Ti-4.5Ni) Fig. 5 (c) and (d) indicated the existence of α-Ti laths, which EDS showed contained little to no Ni in solution. The dark unresolvable domains observed in the optical micrographs of the alloy (Fig. 4 c), were resolved to be eutectoid domains, consisting of Ti_2Ni precipitates in α-Ti. Furthermore, the microstructural features in Alloy 4 (Ti–13Cu-4.5Ni) Fig. 5 (e) and (f) were similar to those in Alloy 2 (Ti–13Cu) in terms of lamellar "pearlitic" regions. However, unlike Alloy 2, the precipitates in Alloy 4 had two grey level contrasts: grey contrasted precipitates, similar to those observed in Alloy 2, and the other light grey brighter precipitates were also observed. EDS analysis quantified the dark-grey precipitates contained about 5 at. %Ni and 27 at. % Cu, indicating they were of the type Ti_2(CuNi)-phase. The Ti_2Cu-phase dissolves up to 13 at.% Ni [47]. The bright white precipitates, which mostly appeared in the "pearlitic" domains contained 11-13 at.%Ni and 8-10 at.% Cu, which were attributable to Ti_4(CuNi), probably a metastable phase in the Ti–Ni–Cu phase system induced by cold pressing and sintering.

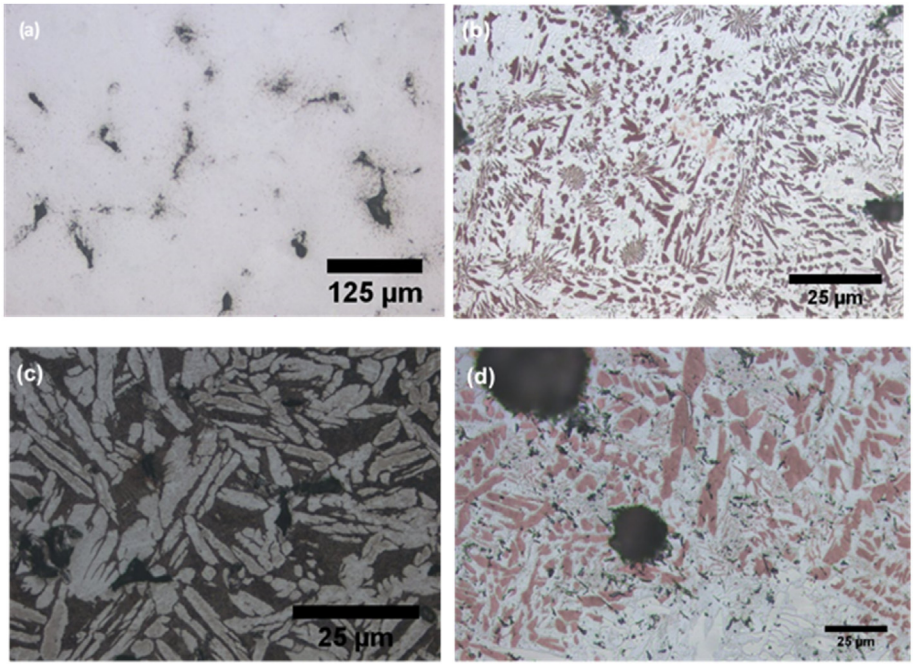

Fig. 4. Optical microstructures of alloys: (a) pure Ti, (b) Ti–13Cu with dendritic precipitates, lamellar and "spherulitic" "pearlitic domains, (c) Ti-4.5Ni with pro-eutectoid α-Ti plates plus dark eutectoid, (d) Ti–13Cu-4.5Ni with lamellar pearlitic domains plus dendritic precipitates.

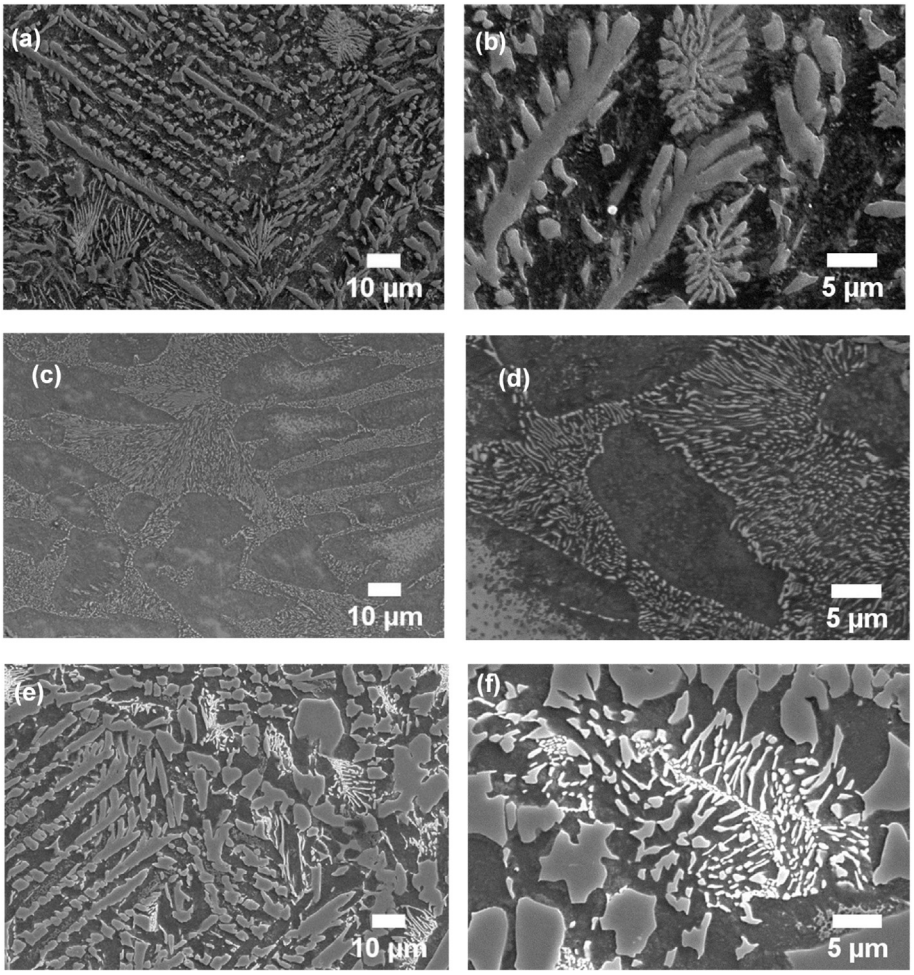

Fig. 5. SEM - SE micrographs of (a & b) Alloy 2 Ti−13Cu, (c & d) Alloy 3 Ti-4.5Ni, and (e & f) Ti−13Cu-4.5Ni.

3.3. XRD pattern analysis

Fig. 6 shows the XRD patterns of the Ti, Ti−13Cu, Ti-4.5Ni, and Ti−13Cu-4.5Ni sintered alloys. The sample containing pure-Ti composed of only an α-Ti phase, in agreement with the microstructures. Alloy 2 (Ti−13Cu) exhibited α-Ti (dominant), Ti_2Cu, and some retained β-Ti phases. It has been previously revealed that Cu induces the β-Ti phase and appears to stabilize β-Ti from as low as 5 wt% Cu [48]. For Alloy 3 (Ti-4.5 Ni), the predominant phase, α-Ti, was observed to coexist with the Ti_2Ni and $TiNi_2$.intermetallic phases The XRD pattern of Ti−13Cu-4.5Ni alloy had peaks for α-Ti, which was the prevalent phase, and peaks for Ti_2Cu, and Ti_2Ni phases. The small β-Ti peak was also observed but it was not very well resolved, as in the case of Alloy 2 (Ti−13Cu), as shown by the corresponding inset in Fig. 6. The observation of retained β-Ti in Alloys 2 and 4 was contrary to some literature, especially on cast Ti−Cu alloys, whereby no retained β-Ti is observed [49]. Retained β-Ti has however been found in PM Ti-5wt%.Cu [48]. The β-phase was retained after sintering and forging processes, with the latter process showing superior mechanical properties [48]. Our results confirm the β-Ti phase in Ti−13Cu and Ti−13Cu-4.5Ni sintered samples. It is possible that cold pressing prior to sintering induced surface deformation that influenced the β-phase formation during sintering [50], hence, this phase is not formed in cast Ti−Cu alloy [28]. At 20 wt % Cu alloying, only the Ti_2Cu precipitated from the α-Ti grains [28] while ~5 wt% Cu induces the β-phase on alloys produced under powder processing [48]. The cold pressing provides deformations on particles surfaces while sintering provides intermediate thermal treatment not sufficient to induce alloy melting. The detected β-Ti phase supports our DSC results showing that both Cu and Ni lowered the α→β phase transformation temperatures possible to be retained upon cooling. This behaviour has been

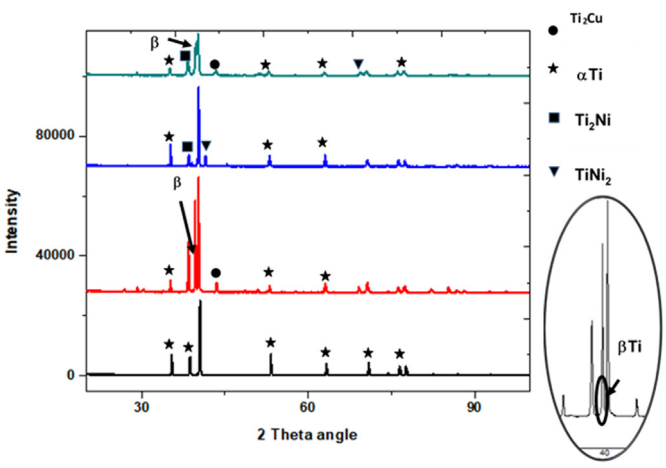

Fig. 6. XRD pattern of pure-Ti, Ti−13Cu, Ti−4.5Ni, and Ti−13Cu−4.5Ni sintered alloys.

observed in pure Ti powder even after been subjected to mechanical deformation [51]. Moreover, it is possible that the high Cu content of 13 wt% acted like the other β-stabilizing elements such niobium (Nb) and trapped the β-phase in Ti alloys [52]. Another possible reason for these differences between cast and PM Ti−Cu alloys could be the differences in the cooling rates the alloys experience from the beta-phase field. Generally, the β→α transformation in titanium is slow [53], and faster cooling rates can lead to a retention of the β phase. The thermal analysis gives a hint on the heat treatment and quenching temperatures of the Ti−13Cu, and Ti−13Cu-4.5Ni sintered alloys to induce the metastable β-phase at room temperature. Such a scenario would be of great interest for the biomedical field as the elastic modulus of the alloy is reduced to be closer to the elastic modulus of the human bone. Such lower elastic modulus would reduce the stress shielding effect that dental implants manufactured with cp Ti grade 4 and Ti−6Al−4V face.

3.4. Grain orientation behaviour

Fig. 7 shows the orientation EBSD maps of the alloys. The band contrast maps of the alloys are shown in Fig. 7a−d, while their phase colour maps are shown in Fig. 7e−h. The pure Ti alloy, Fig. 7a, e, exhibited coarse grains compared to the other alloys, and a homogeneous α-Ti phase. Alloy 2 (Ti−13Cu) possessed a small amount of untransformed β-Ti grains, alongside α-Ti and Ti_2Cu (Fig. 7f) in agreement with the XRD results. The orientation imaging microscopy (OIM) maps of Alloy 3 (Ti-4.5Ni) (Fig. 7c, g) revealed some dark unidentified regions due to surface relief (plateau). These surface plateaus obstructed the detection of diffraction patterns, and as a result, retarded the identification of phases in these areas. However, regions that exhibited Ni-rich grains were distinguished as Ti_2Ni by the EBSD Kikuchi pattern indexation using point analysis, shown in Fig. 8. The microstructure of Alloy 4 (Ti−13Cu-4.5Ni), shown in Fig. 7d, h, had α-Ti, and the intermetallics Ti_2Cu and Ti_2Ni. Both the pro-eutectoid Ti_2Cu laths and the eutectoid nodules of the Ti−13Cu-4.5Ni alloy have relatively increased thickness, compared to the Ti−13Cu alloy. Unlike the XRD data (Fig. 6), untransformed β-Ti was not identified.

Fig. 9 (a)-(d) are the coloured inverse pole figure (IPF) maps of the pure Ti, Ti−13Cu, Ti-4.5Ni, and Ti−13Cu alloys respectively, with their corresponding pole figure maps for the basal (0001), prismatic (10-10) and pyramidal (11−20) planes. Some of the IPF maps show randomly recrystallized grains with a random orientation (randomly mixed) designating no attainable texture, in line with other sintering studies [54]. Only the {0001} poles had maxima, which were fixated around the radial directions, an indication that the data could be attributed to a single α-phase orientation. The texture indices on the {0001} poles had a maximum intensity of ~40, 25, 100, and 25 times random, for the α-Ti based alloys, respectively, while the {11−20}//axial direction (AD) α-fiber texture had a maximum intensity of ~20, 15, 40 and 15 times random, for the pure α-Ti, Ti−13Cu, Ti−45Ni, and Ti−13Cu-4.5Ni alloys, respectively.

Fig. 10 shows the point-to-point misorientation profiles with their correlated cumulative profile relative to the orientation of the original point A, depicted from the IPF maps in Fig. 9 along lines A-B. The cumulative misorientation profiles represent both smooth continuous and discontinuous changes in orientation developed in the sintered alloys. Near point A in Fig. 10a, where the orientation of the grains is smooth and continuous in the cumulative profile, the point-to-point misorientation was less than 0.8º, but the orientation changes and becomes discontinuous in the cumulative profile along with line A-B points (1−3). Generally, points with large point-to-point misorientation exhort to large α/α interface boundaries [55]. Similar trends are observed in Fig. 10b−d, whereby discontinuous orientations demonstrated larger misorientations along line A-B, and on the point-to-point profile, these misorientations were ~0.75º, 1º, 1.5º, for the Ti−13Cu, Ti-4.5Ni, Ti−13Cu-4.5Ni alloys, respectively. However, the local misorientation in all the alloys, were less 15º, the threshold for high angle grain boundaries, when crossing consecutive boundaries. This could be an indication that the grains in the current study were merged in the orientation imaging microscopy (OIM). Therefore, the low angle boundary observed in the α-Ti based alloys is a substantial consequence of microstructural evolution during sintering, and not necessarily a product of texture, which is in agreement with Fig. 9.

In summary, the thermal analysis suggests that with appropriate heat treatment and quenching process above the α→β transition temperatures, the alloy mechanical properties can be improved. The β-phase was confirmed by the EBSD analysis, which supported the XRD analysis by just cold pressing and sintering. This retention of the β-Ti phase in Ti−Cu alloy makes it to be a potential future biomaterial with lower elastic modulus in comparison to pure Ti subject to the further processing of the alloys.

3.5. Density and mechanical properties

Fig. 11 shows the variation of the sintered densities of the alloys in this study. The densities of pure Ti, Ti−13Cu, and Ti-4.5Ni alloys increased on sintering, from (85.8%−90.2%), (87.6%−91.7%), (86.1%−93.2%), respectively. On the other hand, the density of Ti−13Cu-4.5Ni alloy did not change on sintering, indicative of remnant porosity. The introduction of Cu and Ni improved the sintered density compared to the un-alloyed Ti. The increase of the relative sintered density due to Cu has been observed for low content additions of 2 wt% Cu [32] and 5 wt% [56]. In literature, higher Cu additions up to 10 wt% decreased the relative sintered density, compared to low Cu additions due to the formation of a transient liquid at the sintering temperature, which dissolved in the Ti leaving behind pores [32]. In the current study, the Ti-13 wt %Cu sample was sintered at 1200 °C, where there was a persistent liquid phase, which in this case improved densification and the final sintered density. The relative density of the Ti-4.5 wt%Ni alloy was the highest in the current study because Ni has a high diffusivity in Ti, which improves the densification kinetics leading to higher sintered densities [56,57]. The combination of Cu and Ni led to a lower sintered density of the Ti−13Cu-4.5Ni compared to Ti and Ti−13Cu, because of increased porosity, probably caused by the multiple eutectic reactions in the Ti−Cu−Ni alloy evidenced in the DSC analysis.

Table 2 presents the mechanical properties of the alloys investigated. The experimental values with their corresponding corrected error analysis are reported according to John R. Taylor [58]. Typical stress-strain curves of the alloys are shown in Fig. 12. Pure Ti (Alloy 1) had a yield strength (YS) of 350 MPa, ultimate tensile strength (UTS) of 415 MPa, and a remarkably high percentage elongation (%El) to failure of about 10%. The Ti−13Cu has a higher YS in comparison to the Ti-4.5Ni alloy. On the other hand, the simultaneous presence of Cu and Ni in Ti−13Cu-4.5Ni, reduced the YS, compared to Alloy 1 (pure Ti). In general, the alloying elements increased the UTS, while exhibiting lower (%El) to failure, than pure-Ti. The Vickers hardness numbers also increased with alloying: Alloy 1 (pure-Ti) possessed the least hardness of 116 HV, while the hardness values of Alloys 2, 3 and 4 were higher by 41%, 36%, and 47%, respectively.

The increase of YS, UTS and hardness due to the Cu alloying was reported on cast Ti−Cu alloys [59], as well as powder metallurgical processing of Ti−Cu alloys that varied the Cu content to a maximum of Ti-5wt% Cu [48]. As in Alshammari, Yang, & Bolzoni (2019) [28],

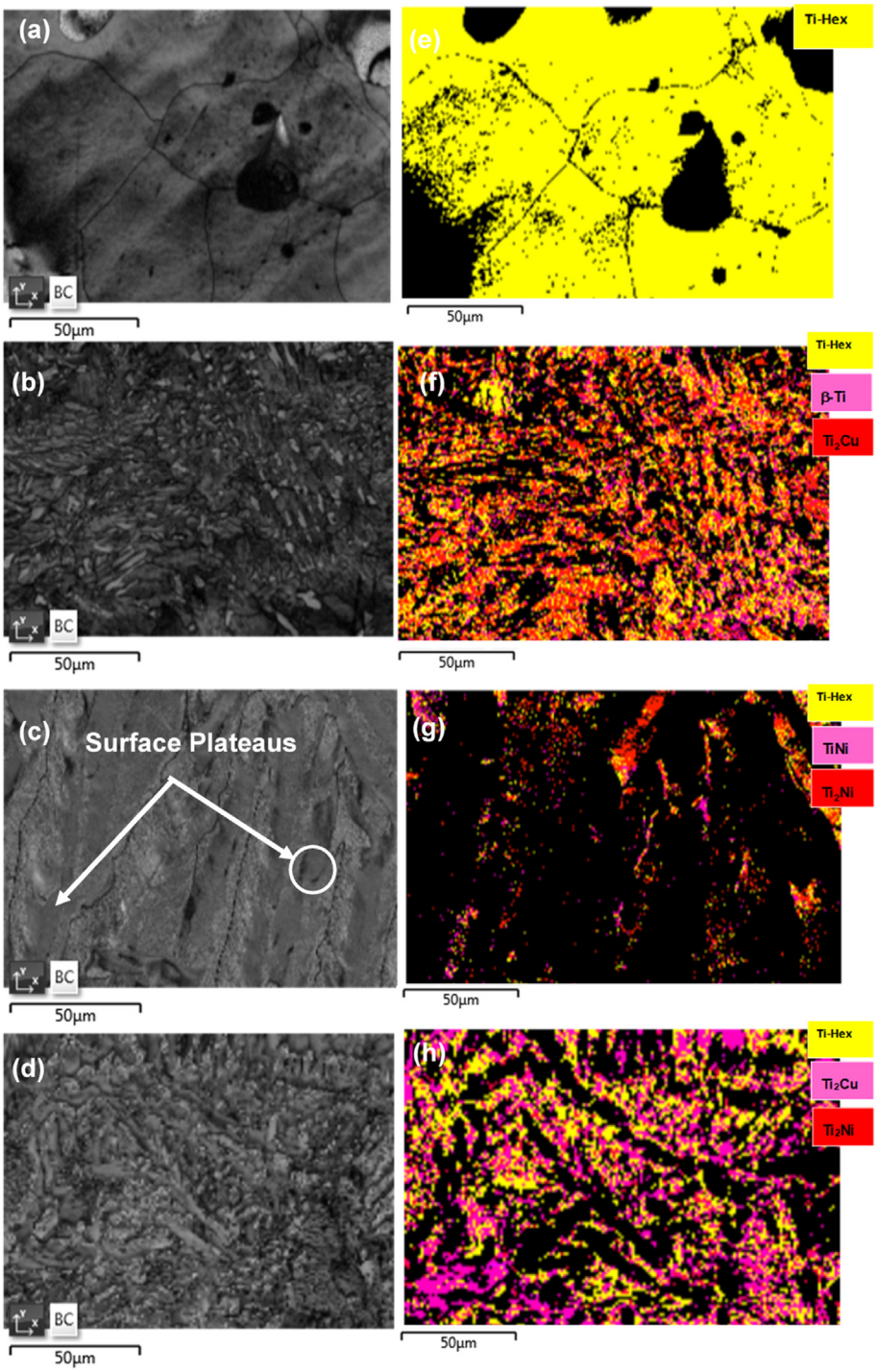

Fig. 7. EBSD data showing: (a)–(d) band contrast maps, and (e)–(h) phase colour orientation maps of the α-Ti, Ti−13Cu, Ti-4.5Ni, and Ti−13Cu-4.5Ni alloys, respectively. (For interpretation of the references to colour in this figure legend, the reader is referred to the Web version of this article.)

the Cu in the current study helped reduce the residual porosity, as seen from the sintered relative densities (Fig. 11) and stabilized some body-centred cubic (bcc) β-Ti phase as shown by XRD analysis (Fig. 6), which has higher strength/hardness with its corresponding low ductility than the hexagonal close-packed (hcp) α-Ti phase. Additionally, the presence of Ti_2Cu intermetallics impede dislocation movement during plastic deformation [60], and therefore strengthen the alloy. For the same reasons, however, the ductility of the alloy reduced drastically to about 40% that of the cp-Ti. However, the ductility was higher than that reported for a cast Ti-10 wt% Cu, and equivalent to that obtained for a cast Ti-5wt% Cu [59] indicating the potential of the powder metallurgical techniques to manufacture useable Ti−Cu alloys. The higher YS, UTS and hardness are due to the Ni alloying resulting in the formation of Ti_2Ni intermetallic precipitates and reduced sample porosity. A direct comparison of the mechanical properties of CP-Ti and low nickel content Ti−Ni powder metallurgy alloys are however rarely reported in the literature. Liu et al. [45], reported a higher hardness

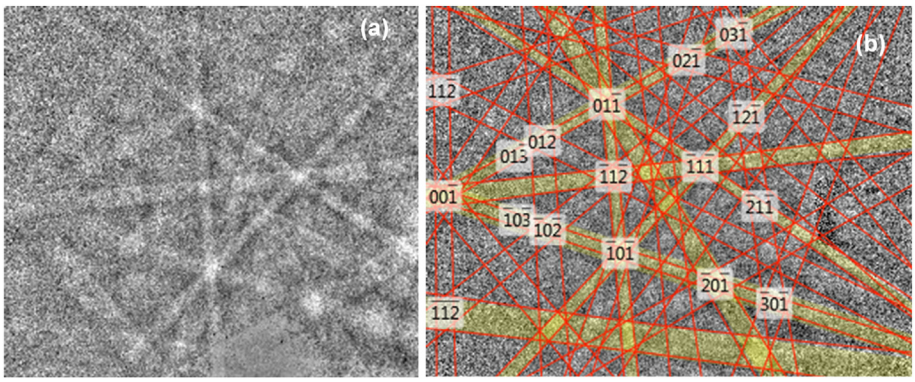

Fig. 8. EBSD Kikuchi patterns of the circled area on Fig. 7c indexed as Ti_2Ni phase (a) Kikuchi pattern and (b) pattern indexation presented in (a).

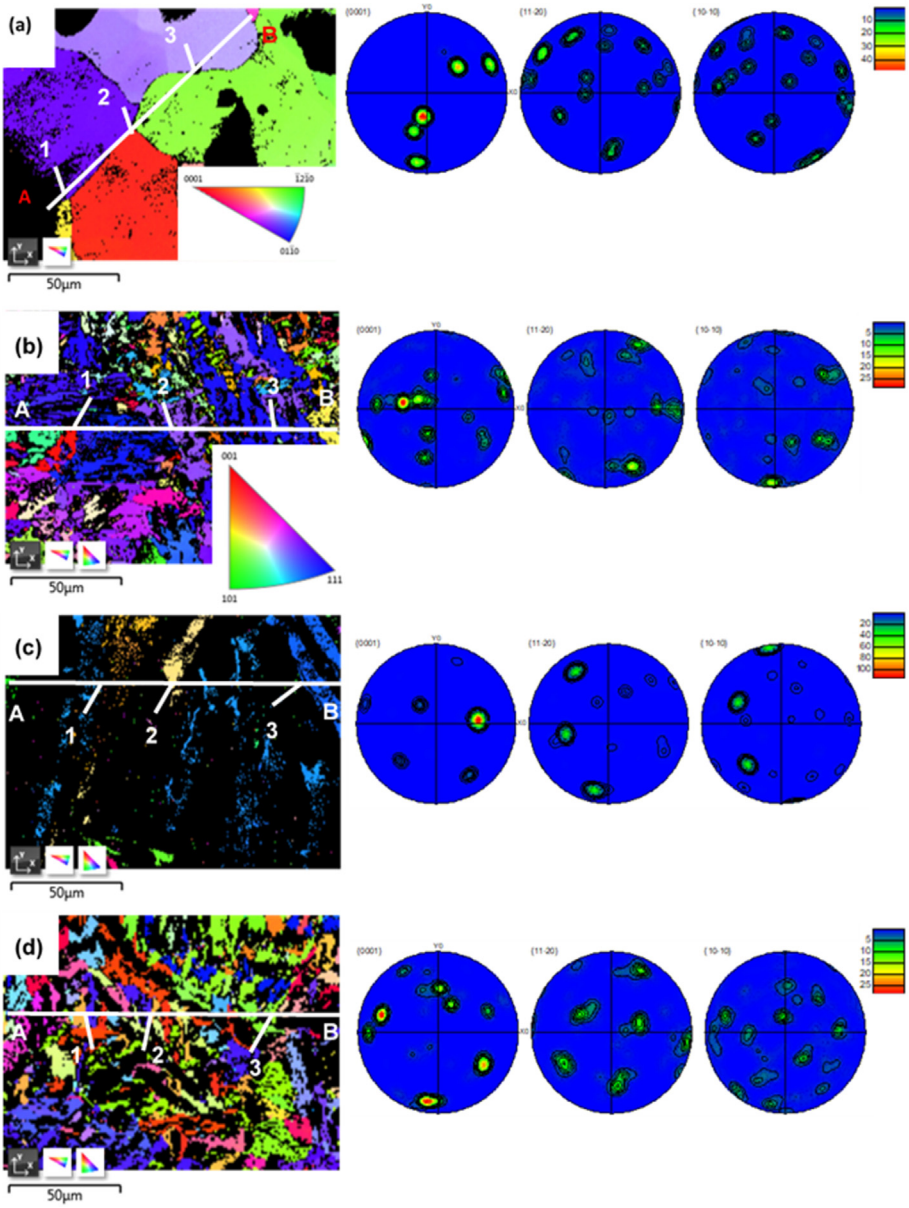

Fig. 9. Inverse pole figure orientation maps of (a) pure-αTi, (b) Ti−13Cu, (c) Ti−4.5Ni, (d) Ti−13Cu−4.5Ni with their corresponding (α-Ti) pole figure maps, respectively.

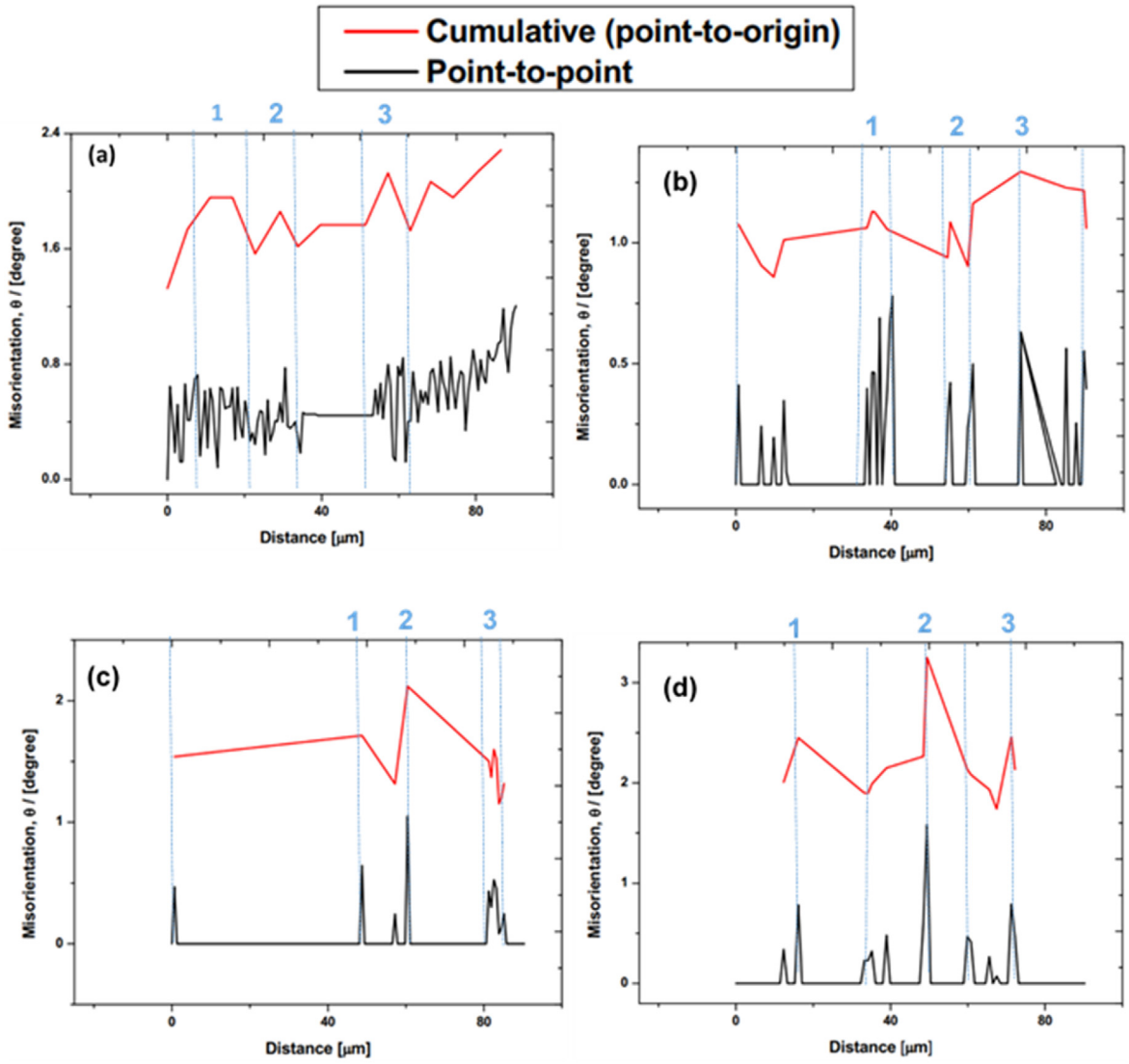

Fig. 10. Misorientation between neighbouring grains (Point-to-point) profiles of the sintered (a) α-Ti, (b) Ti−13Cu, (c) Ti-4.5Ni, and (d) Ti−13Cu-4.5Ni alloys, obtained from the IPF maps along lines A-B (Fig. 9) with their corresponding cumulative misorientation profile relative to the orientation at original point A.

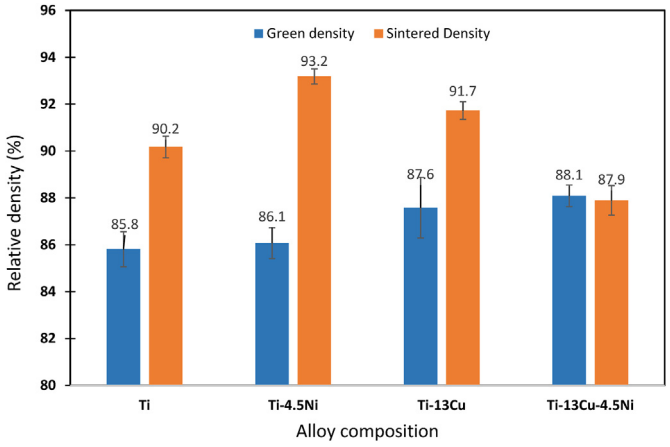

Fig. 11. The green and sintered relative densities of Ti, Ti−13Cu, Ti-4.5Ni and Ti−13Cu-4.5Ni sample alloys. (For interpretation of the references to colour in this figure legend, the reader is referred to the Web version of this article.)

Table 2
Mechanical properties of the sintered Ti-based alloys.

α-Ti alloy	YS (MPa)	UTS (MPa)	Elongation (%)[a]	Vickers hardness
Pure Ti	350 ± 10	415 ± 11	10 ± 2	116 ± 4
Ti−13Cu	540 ± 20	660 ± 20	4 ± 2	195 ± 6
Ti-4.5Ni	480 ± 10	620 ± 10	5 ± 1	180 ± 4
Ti−13Cu-4.5Ni	230 ± 20	460 ± 10	0.3 ± 0.1	220 ± 5

[a] Measured from the difference between final and original lengths of specimens.

and similar or marginally higher YS and UTS than for CP-Ti after sintering Ti-5wt% Ni at 1300 °C. The strengthening mechanisms due to the Ni did not drastically affect the percent elongation to failure. Only the UTS of the Ti−13Cu-4.5Ni alloy was higher than that of cp-Ti, and all the tensile mechanical properties were less than for both the Ti−13Cu and Ti-4.5Ni alloys. This was caused by both the much higher porosity for the Ti−13Cu-4.5Ni alloy, and also the increased strengthening mechanisms discussed for Ti−13Cu and Ti-4.5Ni, respectively. The percent elongation was the lowest primarily due to high porosity. In comparison, the YS, UTS and percent elongation of Ti−13Cu-4.5Ni, at 237 MPa, 464 MPa and

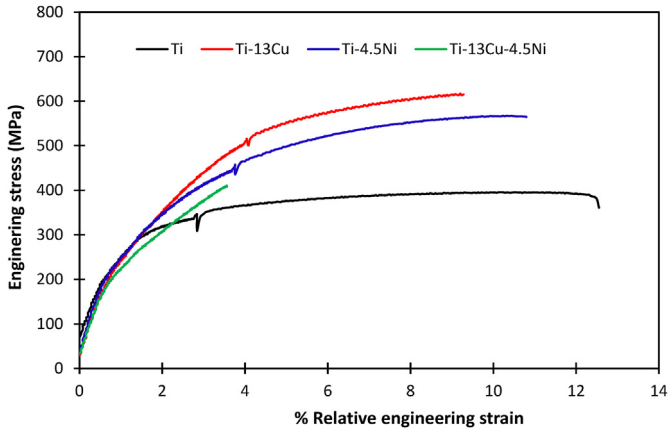

Fig. 12. Characteristic stress-strain behaviour of Ti, Ti−13Cu, Ti-4.5Ni and Ti−13Cu-4.5Ni sample alloys.

0.3%, respectively, are considerably less than those reported in the literature of the cast alloy, i.e. 559 MPa, 703 MPa and 4.1%, respectively [20].

In order to qualify our sintered products for dental applications, their mechanical properties must be comparable to other commercially available dental alloys. Generally, dental alloys are classified according to their yield strength [61]. Type 3 dental casting alloys have a YS $\geq$ 240 MPa, and annealed Type 4 and hardened Type 4 dental casting alloys have a YS $\geq$ 300 MPa and $\geq$450 MPa, respectively, while dental base metal casting alloys have a YS $\geq$ 500 MPa. Based on the YS, the Ti−13Cu, Ti-4.5Ni and Ti−13Cu-4.5Ni alloys produced via powder metallurgy are potentially Type 3 dental alloys. Our alloys meet the requirement of a percent elongation of at least 1.5% for dental base metal casting alloys [62] except for Ti−13Cu-4.5Ni. The Ti−13Cu alloy has a slightly lower UTS and percent elongation (Table 2) when compared with the metal injection (MIM) moulded TiCu alloy comprised of 754 ± 17 MPa and 9.5 ± 1.5% [48]. Furthermore, both Ti−13Cu and Ti-4.5Ni showed comparable properties in comparison to metal injection moulded (MIM) Ti−12Mo (molybdenum) alloy for dental application [63]. For other alloys such as titanium-manganese (Ti−Mn), our alloys are comparable with other properties not considering the effect of porosity [64].

Fig. 13 shows the modes of failure of the tensile test samples. The fracture surfaces of CP-Ti, Ti−13Cu and Ti-4.5Ni in Fig. 13 a-c, are generally distinguished by dimples which is indicative of a ductile fracture. It is worth mentioning that the existence of pores (as pointed by the white arrows) may have influenced the tensile properties of the alloys since pores are the stress concentration areas. The fracture surface of the Ti−13Cu-4.5Ni alloy in Fig. 13d shows the combination of cleavage steps and tongue patterns, indicating a quasi-cleavage brittle fracture. Similar results have been reported elsewhere [65], for an alloy exhibiting low strength and high brittleness. Second particles are also seen on the tearing ridges, which is believed to be stress concentration sites during loading, which act as crack initiation points [66]. Therefore, the resultant low tensile ductility in Alloy 4 was due to the high porosity that predisposed it to easy crack initiation and crack propagation.

4. Conclusion

The effect of Cu, Ni alloying additions on phase transformations, densification, microstructure and tensile behaviour of the conventionally pressed and sintered pure Ti was investigated. The following conclusions were drawn:

- The alloying of Ti with Cu, and Ni to form binary Ti-X alloys leads to higher sintered densities. The Cu promoted liquid phase sintering, while the Ni is a known faster diffuser. However, the ternary alloy Ti−Cu−Ni sintered poorly, probably because of excess liquid at the sintering temperature employed in the study.

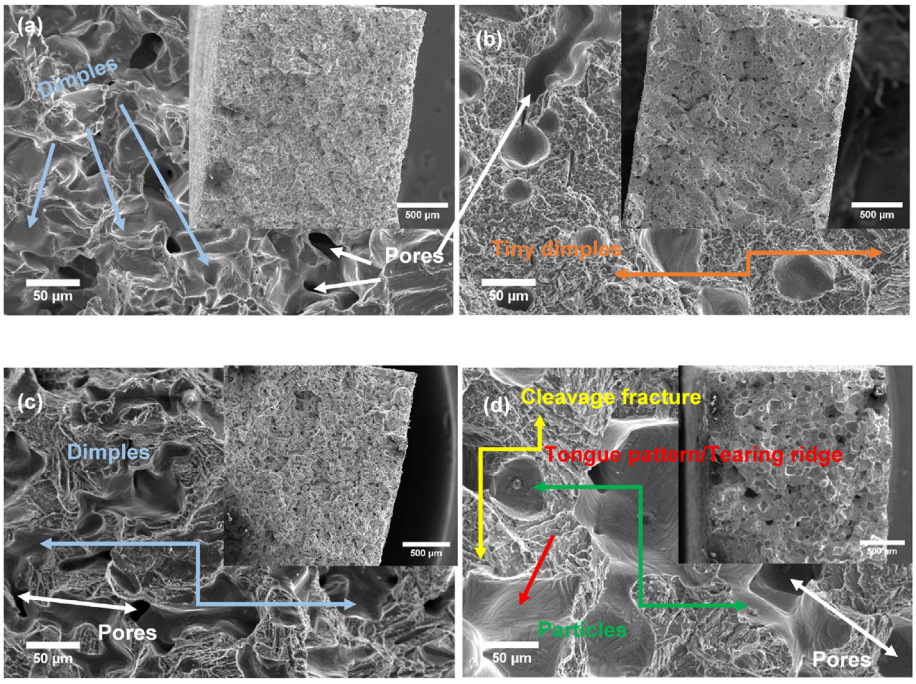

Fig. 13. Fractographic SEM - SE images of the tensile alloy specimens indicating: (a) Pure Ti, (b) Ti−13Cu, (c) Ti-4.5Ni, and (d) Ti−13Cu-4.5Ni, respectively.

- The microstructures of the sintered Ti−Cu and Ti−Cu−Ni are very similar, consisting of dendritic pro-eutectoid Ti_2Cu, and "pearlitic" eutectoid α-Ti and Ti_2Cu. The Ni in the Ti−Cu−Ni alloy dissolved in the Ti_2Cu to form $Ti_2(CuNi)$ precipitates.
- EBSD and orientation image analysis indicated that all the investigated alloys had a similar texture, and together with the thermal behaviour, and XRD analysis, showed that alloys T-13Cu and Ti−Cu−Ni had some retained β−Ti, alongside the α-Ti and precipitated intermetallics. Grain orientation results showed that the low angle boundary observed in the α-Ti grains of the alloys was a substantial consequence of microstructural evolution during sintering at 1200 °C, and not necessarily a product of texture.
- The YS, UTS and hardness of the sintered Ti−13Cu and Ti-4.5Ni alloy were higher than for the sintered Ti, while their %E to failure was less. However, the mechanical properties of the sintered alloys allow them to be classified as either Type 3 dental alloys (Ti), or Type 4 dental alloys (Ti-4.5Ni and Ti−13Cu), indicating that powder metallurgy is a viable manufacturing process for Ti−Cu-based dental alloys.
- The powder metallurgy ternary Ti−13Cu-4.5Ni produced in the current study had inferior properties due to poor sintering that led to the development of extensive porosities. Further work is required to determine whether it can also be sintered with acceptable mechanical properties.

Funding

This work was supported by the Department of Science and Innovation (DSI), Republic of South Africa through the Titanium Centre of Competence (TiCoC), based at the Council for Scientific and Industrial Research (CSIR), Pretoria [Grant number DST/CON 0238; 2015]; and the CSIR's Chief Researcher Grant [Grant number: HCARD08; 2019].

CRediT authorship contribution statement

C. Machio: Conceptualization, Methodology, Writing - review & editing. **M.N. Mathabathe:** Methodology, Writing - original draft, Writing - review & editing. **A.S. Bolokang:** Methodology, Writing - review & editing, Funding acquisition.

Declaration of competing interest

The authors declare that they have no known competing financial interests or personal relationships that could have appeared to influence the work reported in this paper.

Acknowledgements

Authors acknowledge the assistance of Mr. Levy Chauke and Mr. Stephen Masete, of CSIR's Advanced Materials and Engineering's Mechanical Testing Laboratory, with tensile testing. We also thank the University of Pretoria for the EBSD data acquisition.

References

[1] A. Terayama, H. Kyogoku, Shape memory characteristics of the P/M-processed Ti−Ni−Cu alloys, Mater. Sci. Eng. A 527 (21−22) (2010) 5484−5491.
[2] D.C. Ren, H.B. Zhang, Y.J. Liu, S.J. Li, W. Jin, R. Yang, L.C. Zhang, Microstructure and properties of equiatomic Ti−Ni alloy fabricated by selective laser melting, Mater. Sci. Eng. A 771 (2020) 138586.
[3] M. Yamamoto, T. Kuroda, H. Yoneyama, H. Doi, Bending property and phase transformation in Ti-Ni-Cu alloy dental castings for orthodontic application, J. Mater. Sci. Mater. Med. 13 (2002) 855−859.
[4] F. Gok, S.K. Serkan, S. Ozkan, Y.A. Benkli, Comparison of arch width and depth changes and pain/discomfort with conventional and copper Ni-Ti archwires for mandibular arch alignment, J. World Fed. Orthod. 7 (2018) 24−28.
[5] R. Liu, K. Memarzadeh, B. Chang, Y. Zhang, Z. Ma, R.P. Allaker, L. Ren, K. Yang, Antibacterial effect of copper-bearing titanium alloy (Ti-Cu) against Streptococcus mutans and Porphyromonas gingivalis, Sci. Rep. (2016) 1−10.
[6] E. Zhang, X. Wang, M. Chen, B. Hou, Effect of the existing form of Cu element on the mechanical properties, bio-corrosion and antibacterial properties of Ti-Cu alloys for biomedical application, Mater. Sci. Eng. C 69 (2016) 1210−1221.
[7] E. Zhang, L. Zheng, J. Liu, B. Bai, C. Liu, Influence of Cu content on the cell biocompatibility of Ti-Cu sintered alloys, Mater. Sci. Eng. C 46 (2015) 148−157.
[8] R.G. Craig, C.T. Hanks, Reaction of fibroblasts to various dental casting alloys, J. Oral Pathol. 17 (1988) 341−347.
[9] E. Zhang, S. Li, J. Ren, L. Zhang, Y. Han, Effect of extrusion processing on the microstructure, mechanical properties, biocorrosion properties and antibacterial properties of Ti-Cu sintered alloys, Mater. Sci. Eng. C 69 (2016) 760−768.
[10] M.J. Phasha, A.S. Bolokang, P.E. Ngoepe, Solid-state transformation in nanocrystalline Ti induced by ball milling, Mater. Lett. 64 (2010) 1215−1218.
[11] A.S. Bolokang, M.J. Phasha, Thermal analysis on the curie temperature of nanocrystalline Ni produced by ball milling, Adv. Pow. Technol. 22 (2011) 518−521.
[12] H.H. Huang, Surface characterizations and corrosion resistance of nickel- titanium orthodontic archwires in artificial saliva of various degrees of acidity, J. Biomed. Mater. Res. 74 (2005) 629−639.
[13] M. Geetha, A.K. Singh, R. Asokamani, A.K. Gogia, Ti based biomaterials, the ultimate choice for orthopaedic implants−A review, Prog. Mater. Sci. 54 (2009) 397−425.
[14] J.D. Bumgardner, L.C. Lucas, Cellular response to metallic ions released from nickel-chromium dental alloys, J. Dent. Res. 74 (1995) 1521, https://doi.org/10.1177/00220345950740081401.
[15] D.-Y. Kim, C.-M. Kim, J.-H. Kim, H.-Y. Kim, W.-C. Kim, Evaluation of marginal and internal gaps of Ni-Cr and Co-Cr alloy copings manufactured by micro-stereolithography, J. Adv. Prosthodont. 9 (2017) 176−181.
[16] J.C. Setcos, A. Babaei-Mahani, L. Di Silvio, A.M. Nairn, H.F. Wilson, The safety of nickel containing dental alloys, Dent. Mater. 22 (2006) 1163−1168.
[17] M. Arndt, A. Bruck, T. Scully, A. Jager, C. Bourauel, Nickel ion release from orthodontic NiTi wires under simulation of realistic in-situ conditions, J. Mater. Sci. 40 (2005) 3659−3667.
[18] T. Eliades, E.A. Arthanasiou, In Vivo aging of orthodontic alloys: Implications for corrosion potential, nickel release, and biocompatibility, Angle Orthod. 72 (2002) 222−237.
[19] Y. Alshammari, M. Jia, F. Yang, L. Bolzoni, The effect of α+β forging on the mechanical properties and microstructure of binary titanium alloys produced via a cost-effective powder metallurgy route, Mater. Sci. Eng. A 769 (2020) 138496.
[20] R. Waterstrat, Comments on casting of Ti-13Cu-4.5Ni alloy, DHEW 77−1 (1977) 224−233. NIH.
[21] H.F. Li, K.J. Qiu, F.Y. Zhou, L. Li, Y.F. Zheng, Design and development of novel antibacterial Ti-Ni-Cu shape memory alloys for biomedical application, Sci. Rep. 6 (2016), https://doi.org/10.1038/srep37475.
[22] H.B. Bomberger, G.S. Hall, S.R. Seagle, Low melting hypereutectoid titanium-copper alloys, in: Titan. '80, Sci. Technol. Proc. Fourth Int. Conf. Titanium, 1980. https://ci.nii.ac.jp/naid/80001055029/en.
[23] A. Fraker, A. Ruff, P. Sung, A. van Orden, K. Speck, Surface preparation and corrosion behavior of titanium alloys for surgical implants, in: H. Luckey, F. Kubil (Eds.), ASTM International, 1983, pp. 206−219. West Conshohocken, PA.
[24] W.M. Elshahawy, I. Watanabe, P. Kramer, In vitro cytotoxicity evaluation of elemental ions released from different prosthodontic materials, Dent. Mater. 25 (2009) 1551−1555.
[25] N. Mitsuo, Mechanical properties of biomedical titanium alloys, Mater. Sci. Eng. A 243 (1998) 231−236.
[26] K. Ida, Titanium, from mining to biomaterials, in: The Wollongong Symposium, 1991, pp. 63−71.
[27] M. Kikuchi, Y. Takada, S. Kiyosue, M. Yoda, M. Woldu, Z. Cai, O. Okuno, Mechanical properties and microstructures of cast Ti-Cu alloys, Dent. Mater. 19 (2003) 174−181.
[28] Y. Takada, H. Nakajima, O. Okuno, T. Okabe, Microstructure and corrosion behavior of binary titanium alloys with beta-stabilizing elements, Dent. Mater. 20 (2001) 34−52.
[29] E. Zhang, F. Li, H. Wang, J. Liu, C. Wang, M. Li, K. Yang, A new antibacterial titanium-copper sintered alloy: Preparation and antibacterial property, Mater. Sci. Eng. C 33 (7) (2013) 4280−4287.
[30] J. Liu, F. Li, C. Liu, H. Wang, B. Ren, K. Yang, E. Zhang, Effect of Cu content on the antibacterial activity of titanium-copper sintered alloys, Mater. Sci. Eng. C 35 (1) (2014) 392−400.
[31] Z. Ahmadi, B. Nayebi, M. Asl, Shahedi, M.G. Kakroudi, Fractographical characterization of hot pressed and pressureless sintered AlN-doped ZrB2−SiC composites, Mater. Charact. 110 (2015) 77−85.
[32] T. Luangvaranunt, P. Pripanapong, Pin-on-disc wear of precipitation hardened titanium copper alloys fabricated by powder metallurgy, Mater. Trans. 53 (3) (2012) 518−523.
[33] Y.-H. Li, N. Chen, H.-T. Cui, F. Wang, Fabrication and characterization of porous Ti-10Cu alloy for biomedical application, J. Alloy. Compd. 723 (2017) 967−973.

[34] M. Kikuchi, M. Takahashi, O. Okuno, Elastic moduli of cast Ti-Au, Ti-Ag, and Ti-Cu alloys, Dent. Mater. 22 (7) (2006) 641–646.
[35] X. Liu, S. Chen, J.K.H. Tsoi, J.P. Matinlinna, Binary titanium alloys as dental implant materials—a review, Regen. Biomater. (2017) 315–323, https://doi.org/10.1093/rb/rbx027.
[36] A.S. Bolokang, M.N. Mathabathe, C. Mathebula, C.N. Machio, Thermal analysis and morphology of the ball-milled Ti-Ni powder, Mater. Today Proc. (2020) 1–5, https://doi.org/10.1016/j.matpr.2020.02.351.
[37] M.N. Mathabathe, A.S. Bolokang, G. Govender, C.W. Siyasiya, R.J. Mostert, Cold-pressing and vacuum arc melting of γ-TiAl based alloys, Adv. Powder Technol. 30 (12) (2019) 2925–2939.
[38] M.N. Mathabathe, A.S. Bolokang, G. Govender, R.J. Mostert, C.W. Siyasiya, Structure-property orientation relationship of a $\gamma/\alpha_2/Ti_5Si_3$ in as-cast Ti-45Al-2Nb-0.7Cr-0.3Si intermetallic alloy, J. Alloys Compd. 765 (2018) 690–699.
[39] M. Turchanin, P. Agraval, A. Fesenko, Thermodynamics of liquid alloys and metastable phase transformations in the copper–titanium system, Powder Metall. Met. Ceram. 44 (5–6) (2005) 257–270.
[40] G. Franti, J. Williams, H. Aaronson, A survey of eutectoid decomposition in ten Ti-X systems, Metall. Trans. A 9A (1978) 1641–1649.
[41] D. Bandyopadhyay, R.C. Sharma, N. Chakraborti, The Ti-Ni-C system (Titanium-Nickel-Carbon), J. Phase Equilib. 21 (2) (2000) 186–191.
[42] K. Gupta, The Cu-Ni-Ti (Copper-Nickel-Titanium) system, J. Phase Equilib. 23 (6) (2002) 541–547.
[43] C. Gabriele, J. Schuster, Cu-Ni-Ti (Copper-Nickel-Titanium). Light Metal Ternary Systems: Phase Diagrams, Crystallogr. Thermodyn. Data, 2005, pp. 266–283.
[44] Y. Masao, K. Yoshiyuki, K. Kiyoshi, Phase equilibria in the Ti corner of the Ti–Ni–Cu system, J. Jpn. Inst. Met. 46 (6) (1982) 571–577.
[45] H.-W. Liu, D. Bishop, K. Plucknett, A comparison of Ti–Ni and Ti-Sn binary alloys processed using powder metallurgy, Mater. Sci. Eng. A 644 (2015) 392–404.
[46] H. Donthula, B. Vishwanadh, T. Alam, T. Borkar, R.J. Contieri, R. Caram, Morphological evolution of transformation products and eutectoid transformation(s) in a hyper-eutectoid Ti-12 at % Cu alloy, Acta Mater. 168 (2019) 63–75.
[47] V. Loo, B. Leenen, Phase relations in the ternary Ti-Ni-Cu system at 800 and 870°C, J. Less Common Met. 57 (1978) 111–121.
[48] Y. Alshammari, F. Yang, L. Bolzoni, Low-cost powder metallurgy Ti-Cu alloys as a potential antibacterial material, J. Mech. Behav. Biomed. Mater. 95 (2019) 232–239.
[49] Y. Takada, H. Nakajima, O. Okuno, T. Okabe, Microstructure and corrosion behavior of binary titanium alloys with beta-stabilizing elements, Dent. Mater. J. 20 (1) (2001) 34–52.
[50] S.T. Camagu, N.M. Mathabathe, D.E. Motaung, T.F.G. Muller, C.J. Arendse, A.S. Bolokang, Investigation into the thermal behaviour of the B2–NiAl intermetallic alloy produced by compaction and sintering of the elemental Ni and Al powders, Vacuum 169 (2019) 108919.
[51] A.S. Bolokang, D.E. Motaung, C.J. Arendse, T.F.G. Muller, Formation of the metastable FCC phase by ball milling and annealing of titanium-stearic acid powder, Adv. Powder Technol. 26 (2) (2015) 632–639.
[52] C. Mathebula, W. Matizamhuka, A.S. Bolokang, Effect of Nb content on phase transformation, microstructure of the sintered and heat-treated Ti (10–25) wt.% Nb alloys, Int. J. Adv. Manuf. Technol. (2020), https://doi.org/10.1007/s00170-020-(2020)05385-9.
[53] T. Okabe, H. Hero, The use of titanium in dentistry, Cells Mater. 5 (2) (1995) 211–230.
[54] R. Xu, B. Liu, Z. Yan, F. Chen, W. Guo, Y. Liu, Low-cost and high-strength powder metallurgy Ti–Al–Mo–Fe alloy and its application, J. Mater. Sci. 54 (2019) 12049–12060.
[55] Y. Ito, S. Murakami, N. Tsuji, SEM/EBSD analysis on globularization behavior of lamellar microstructure in Ti-6Al-4V during hot deformation and annealing, Metall. Mater. Trans. A Phys. Metall. Mater. Sci. 48A (9) (2017) 4237–4246.
[56] I.M. Robertson, G.B. Schaffer, Design of titanium alloy for efficient sintering to low porosity, Powder Metall. 52 (4) (2009) 311–315.
[57] B. Panigrahi, Sintering behaviour of Ti–2Ni and Ti–5Ni elemental powders, Mater. Lett. 61 (2007) 152–155.
[58] J.R. Taylor, Introduction to Error Analysis: the Study of Uncertainties in Physical Measurements, University Science Books, 1997.
[59] K. Takada, K. Yoda, W. Cai, O. Okabe, Mechanical properties and microstructures of cast Ti-Cu alloys, Dent. Mater. 19 (2003) 174–181.
[60] A. Lawan, M. Brendon, E. Nifise, B. Joseph, P. Fortinate, P. Apata, Effect of nickel addition on densification , microstructure and wear behaviour of spark plasma sintered CP-titanium, Mater. Chem. Phys. 240 (2020) 122130.
[61] M. Takahashi, M. Kikuchi, Y. Takada, O. Okuno, Mechanical properties and microstructures of dental cast Ti-Ag and Ti-Cu alloys, J. Dent. Mater. 21 (2002) 270–280.
[62] Ansi/Ada, Dental Base Metal Casting Alloys, ADA14-1982D, Illinois, 1998, pp. 1–10.
[63] W. Xu, X. Lu, L. Wang, Z.M. Shi, S.M. Lv, M. Qian, X.H. Qu, Mechanical properties, in vitro corrosion resistance and biocompatibility of metal injection molded Ti-12Mo alloy for dental applications, J. Mech. Behav. Biomed. Mater. 88 (2018) 534–547.
[64] Y. Alshammari, F. Yang, L. Bolzoni, Mechanical properties and microstructure of Ti-Mn alloys produced via powder metallurgy for biomedical applications, J. Mech. Behav. Biomed. Mater. 91 (2019) 391–397.
[65] Y. Zhao, W. Wang, K. Yan, C. Liu, J. Zou, Microstructure and properties of Cu/Ti laser welded joints, J. Mater. Process. Tech. 257 (2018) 244–249.
[66] X. Yi, G. Wen, K. Sun, W. Gao, H. Wan, B. Sun, X. Meng, W. Cai, L. Zhao, Fabrication , characterization and potential application of larger bulk Ti-Ni-Hf high temperature shape memory alloy composite reinforced by hybrid particles, J. Alloys Compd. 764 (2018) 347–358.